HOKKAIDO UNIVERSITY

Title	Infrared Spectra of Monohydrogenated Aniline, ortho- and para-HC6H5NH2, Generated in Solid para-Hydrogen
Author(s)	Tsuge, Masashi; Chen, Yu-Hsuan; Lee, Yuan-Pern
Citation	Journal of physical chemistry A, 124(37), 7500-7510 https://doi.org/10.1021/acs.jpca.0c06079
Issue Date	2020-09-17
Doc URL	https://hdl.handle.net/2115/82682
Rights	This document is the Accepted Manuscript version of a Published Work that appeared in final form in The Journal of Physical Chemistry A, copyright c American Chemical Society after peer review and technical editing by the publisher. To access the final edited and published work see https://pubs.acs.org/doi/10.1021/acs.jpca.0c06079.
Type	journal article
File Information	HydrogenatedAniline-rev.pdf



Hokkaido University Collection of Scholarly and Academic Papers : HUSCAP

Infrared Spectra of Mono-hydrogenated Aniline, *ortho*- and *para*-$HC_6H_5NH_2$, Generated in Solid *para*-Hydrogen

Masashi Tsuge, *[†,‡] Yu-Hsuan Chen,[†] and Yuan-Pern Lee*[†,§,⊥]

[†] *Department of Applied Chemistry and Institute of Molecular Science, National Chiao Tung University, Hsinchu 300093, Taiwan*
[‡] *Institute of Low Temperature Sciences, Hokkaido University, Sapporo 060-0819, Japan*
[§] *Center for Emergent Functional Matter Science, National Chiao Tung University, Hsinchu 300093, Taiwan*
[⊥] *Institute of Atomic and Molecular Sciences, Academia Sinica, Taipei 106319, Taiwan*

* Corresponding authors
E-mail address: tsuge@lowtem.hokudai.ac.jp (M. Tsuge).
E-mail address: yplee@nctu.edu.tw (Y.-P. Lee).
Full postal address: 1001 Ta-Hsueh Road, Hsinchu 300093, Taiwan (Y.-P. Lee).

KEYWORDS
Infrared spectroscopy, matrix isolation, para-hydrogen, hydrogenated aniline

ABSTRACT: The isomers of mono-hydrogenated aniline ($HC_6H_5NH_2$) are regarded as important intermediates in reduction reactions of aniline, but their spectral identification has been limited to electron paramagnetic resonance in an adamantane matrix. We report here infrared spectra of two least-energy isomers of $HC_6H_5NH_2$, produced on electron bombardment during deposition of a matrix of aniline and *para*-hydrogen at 3.2 K. The intensities of IR lines of $HC_6H_5NH_2$ increased during maintenance of the electron-bombarded matrix in darkness for a prolonged period because of the neutralization of protonated aniline, $H^+C_6H_5NH_2$, by trapped electrons and further reactions between aniline and the unreacted hydrogen atoms that were produced during electron bombardment. The observed lines were grouped according to their behaviors on secondary photolysis with light at 520, 465, and 375 nm. On comparison of experimental spectra with quantum-chemically predicated spectra for four possible isomers of $HC_6H_5NH_2$, lines in one group were assigned to the most stable *ortho*-$HC_6H_5NH_2$ and those in the other group were assigned to the second most stable *para*-$HC_6H_5NH_2$. Their photolytic behaviors at varied wavelengths are consistent with predicted UV-absorption bands. The mechanisms of formation of these isomers are discussed according to semi-quantitative analysis.

1. INTRODUCTION

Aniline ($C_6H_5NH_2$), the simplest amino-substituted benzene, is widely used in chemical synthesis of rubber materials, dyeing agents, and pharmaceuticals. An important chemical reaction of substituted benzene (C_6H_5X) is the Birch reduction,[1-3] in which the benzene ring is partially reduced to give substituted, unconjugated 1,4-cyclohexadiene, in contrast to catalytic reductions that typically generate substituted cyclohexane. The Birch rule,[4] which predicts a kinetic preference for that regioisomers with the maximum number of substituents on the residual double bonds, has been quite successful. In the Birch reduction of substituted benzene, a substituted cyclohexadienyl radical (**3**) appears as an intermediate (Scheme 1). The preferred site of protonation in the rate-determining second step (**2** → **3**) has been debated;[5-8] even though the final product (**5**) would be the same, whether the intermediate (**3**) is hydrogenated at the *ortho*- or *meta*-position with respect to the substituent is unclear. Early computational studies indicated that the intermediate could be hydrogenated at either the *ortho*- or the *meta*-position.[5-7] However, Zimmerman and Wang reported that, according to experiments, the *ortho*-position is much preferred for hydrogenation in the Birch reduction of anisole (X = OCH_3), toluene (X = CH_3), and other derivatives.[8] In situ detection of reaction intermediates will give strong evidence for the confirmation of mechanism, but spectral information on them (i.e., hydrogenated substituted benzene) are quite limited.

The hydrogenation of benzene to form C_6H_7 has been well studied. The infrared spectra of C_6H_7 and C_6H_6D in solid *p*-H_2 clearly indicated that the observed species is a cyclohexadienyl radical, the so-called σ-complex.[9] Spectral studies of the structural identification of mono-hydrogenated substituted benzene radical are, however, few. To our knowledge, for mono-hydrogenated aniline ($HC_6H_5NH_2$), only an electron-paramagnetic resonance (EPR) spectrum of the amino-cyclohexadienyl radical was reported by DiGregorio et al., who produced this radical through X-ray irradiation of aniline in an adamantane matrix.[10] These authors found that $C_6H_5NH_2$ is hydrogenated dominantly at the *ortho*-site and with a small contribution at the *para*-site. Hydrogenation of aniline might occur at four distinct positions-- *ipso*-, *ortho*-, *meta*-, and *para*-sites, designated as *ipso*-, *ortho*-, *meta*-, and *para*-$HC_6H_5NH_2$ in this paper. Obtaining further spectral information about these isomers is important

in understanding the related reaction mechanism.

Para-hydrogen (p-H_2) has emerged as a new matrix host suitable for producing hydrogenated species.[11-12] Two techniques employed in generating hydrogenated species in solid p-H_2 are photolysis *in situ* of precursors producing hydrogen atoms and the electron bombardment of a p-H_2 matrix during its deposition. In the former method, UV photolysis of a p-H_2 matrix containing trace of Cl_2 was commonly used to produce isolated Cl atoms that further reacted with vibrationally excited H_2 molecule upon IR irradiation (> 4000 cm^{-1}) to produce hydrogen atoms.[13] The hydrogen atoms thus produced diffused in solid p-H_2 through the breaking and formation of H–H bonds so that they have better chance to react with embedded molecules than with only nearest neighbors. Even if the hydrogenation has a small barrier, it might occur via quantum-mechanical tunneling. Hence, an isomer with the smallest barrier tends to be produced in this method. In the latter method, electron bombardment of p-H_2 during matrix deposition produces proton (H_3^+) and hydrogen atom, which react with the guest molecule to produce protonated and hydrogenated species. The neutralization of protonated species is expected also to contribute to the production of hydrogenated species. A greater variety of hydrogenated isomers might hence be produced, compared with the photolytic method. The spectral lines of protonated and hydrogenated species could be readily distinguished because reactions such as trapped electrons with the protonated species destroyed the protonated species and produced the hydrogenated species during maintenance of the matrix in darkness for a prolonged period. For both methods, the hydrogenation typically stops at the first step because, with a limited amount of H atoms and with the mixing ratio of the parent much greater than that of the mono-hydrogenated radicals, further hydrogenation cannot compete with the first hydrogenation step. The electron-bombardment method has been used to identify several hydrogenated aromatic species, including benzene derivatives,[9, 14] heterocyclic compounds,[12, 15] and polycyclic aromatic hydrocarbons. [16-20]

We have reported the IR spectra of three isomers of protonated aniline, *para*-, *amino*-, and *ortho*-$H^+C_6H_5NH_2$, produced on electron bombardment of an aniline/p-H_2 matrix;[21] these spectral lines decreased in intensity during maintenance of the matrix in darkness for a prolonged period. Here we report the assignments of those lines produced on electron bombardment of an aniline/p-H_2 matrix of

which the intensities increased during maintenance of the matrix in darkness to the two most stable isomers of hydrogenated aniline, *ortho*- and *para*-$HC_6H_5NH_2$.

2. EXPERIMTNAL AND COMPUTATIONAL METHODS

The experimental setup for infrared spectrometry and *p*-H_2 matrix isolation coupled with electron bombardment has been described elsewhere.[9] A gold-plated copper block, cooled to 3.2 K with a closed-cycle helium refrigerator, served as a matrix substrate and as a mirror to reflect the incident IR beam to the detector for reflective absorption measurements. Infrared absorption spectra were recorded with a Fourier-transform infrared (FTIR) spectrometer equipped with a KBr beam splitter and a HgCdTe detector cooled to 77 K. Two hundred scans for spectral range 5000–450 cm^{-1} at resolution 0.25 cm^{-1} were typically acquired at each stage of the experiment.

The gaseous mixtures of $C_6H_5NH_2$ and *p*-H_2 were bombarded with electrons during deposition at 3.2 K. A beam of electrons with kinetic energy 200 eV and current 30 μA was provided by an electron gun (Kimball Physics, EFG-7). We used a mixture $C_6H_5NH_2$/*p*-H_2 with typical mixing ratio of 70 ppm. This mixture was deposited at a rate of 13 mmol h^{-1} over a period of 8–10 h. After deposition, the matrix was maintained in darkness for a prolonged period to differentiate various products. Secondary photolysis experiments were performed subsequently using light at 520±10, 465±10, and 375±10 nm from light-emitting diodes.

Preparation of a pure *p*-H_2 sample has been described previously.[9, 22] Conversion temperatures 12–13 K yielded *p*-H_2 samples that contain less than 100 ppm *ortho*-H_2. Pure *p*-H_2 gas thus obtained was mixed with $C_6H_5NH_2$ vapor in a vacuum manifold. Before mixing, the commercially obtained $C_6H_5NH_2$ (Aldrich, ≥99.5 %) was degassed with several freeze-pump-thaw cycles.

Quantum-chemical calculations were performed with programs Gaussian 09 (Rev. E.01) and Gaussian 16 (Rev. B.01).[23-24] The density-functional theory with the B3LYP functional[25-26] and Dunning's correlation-consistent basis set, cc-pVTZ,[27] were employed to perform geometry optimizations and harmonic vibrational analyses. Anharmonic vibrational wavenumbers were also obtained with the second-order vibrational perturbation theory (VPT2) implemented in the Gaussian

09 program.[28] For the calculation of single-point energies, the zero-point vibrational energy (ZPVE) was corrected with harmonic vibrational wavenumbers without scaling. Calculations of UV-Vis spectra were performed with time-dependent density-functional theory (TD-DFT)[29] with CAM-B3LYP functionals.[30]

3. COMPUTATIONAL RESULTS

3.1 Geometry and relative energies

As mentioned above, aniline has four possible sites for hydrogenation: *para*-, *meta*-, *ortho*-, and *ipso*-positions. The geometries of these isomers of mono-hydrogenated aniline optimized with the B3LYP/cc-pVTZ method are presented in Figure 1; the carbon atoms are numbered. *para*-$HC_6H_5NH_2$ possesses point-group symmetry C_s; other isomers belong to point group C_1. Hydrogenation distorts the planar phenyl ring slightly, as evident from the changes in inner angles (for example, $\angle C^{(1)}C^{(2)}C^{(3)}$ = 113.6° in *ortho*-$HC_6H_5NH_2$); the out-of-plane distortion is negligible. The $C^{(1)}$–N bond length in *ortho*- and *meta*-$HC_6H_5NH_2$ varied by ~0.01 Å from that (1.395 Å) of aniline, whereas that in *ipso*-$HC_6H_5NH_2$ increased by ~0.1 Å due to the change in hybridization of the carbon atom. The NH_2 group is slightly tilted towards the hydrogenated side in *ortho*- and *meta*-$HC_6H_5NH_2$.

As summarized in Table 1, *ortho*-$HC_6H_5NH_2$ has the least energy and *para*-, *meta*-, and *ipso*-$HC_6H_5NH_2$ have energies greater by 9.8, 14.2, and 42.0 kJ mol^{-1}, respectively; these energies are corrected for ZPVE. The transition states (TS) for hydrogenation and isomerization reactions were also calculated; the potential-energy scheme for the H + $C_6H_5NH_2$ system is depicted in Figure 2. The hydrogenation to form *ipso*-$HC_6H_5NH_2$ has the largest barrier, 38.3 kJ mol^{-1}, whereas those paths to form other isomers have barriers in a much smaller range, 9.8–15.0 kJ mol^{-1}. The energies of the transition states (TS1–TS3) for isomerization, 195–225 kJ mol^{-1}, are much greater than that of H + $C_6H_5NH_2$, indicating that these isomerization reactions are unlikely to occur.

3.2 Predicted vibrational spectra

Scaled harmonic vibrational wavenumbers and IR intensities predicted with the B3LYP/cc-pVTZ

method are listed in Tables 2, 3, S-1, and S-2 for *ortho*-, *para*-, *meta*-, and *ipso*-$HC_6H_5NH_2$, respectively. The calculated harmonic vibrational wavenumbers are scaled according to equations $y = (0.9212 \pm 0.031)\,x + (138 \pm 101)$ and $y = (0.9716 \pm 0.004)\,x + (8.5 \pm 4.6)$ for values above and below 2000 cm^{-1}, respectively, in which y is the scaled values and x is the calculated harmonic vibrational wavenumber. These equations, derived according to a linear relation between predicted harmonic vibrational wavenumbers and observed wavenumbers of $C_6H_5NH_2$ isolated in a *p*-H_2 matrix,[21] are employed for other species discussed in this work. Anharmonic vibrational wavenumbers and IR intensities are also listed in these tables for comparison.

Several intense vibrational lines are predicted to be associated with the NH_2 and CH_2 groups of $HC_6H_5NH_2$. We describe here the characteristic vibrational modes of the two most stable isomers, *ortho*- and *para*-$HC_6H_5NH_2$, and list scaled harmonic vibrational wavenumbers unless otherwise indicated. For *ortho*-$HC_6H_5NH_2$, antisymmetric (ν_1) and symmetric (ν_2) NH_2 stretching modes are predicted at 3495 and 3399 cm^{-1}, which are slightly red-shifted from those of aniline, predicted at 3504 and 3415 cm^{-1}. Further red shifts are predicted for *para*-$HC_6H_5NH_2$, of which the wavenumbers of antisymmetric (ν_{23}) and symmetric (ν_1) NH_2-stretching modes are 3489 and 3397 cm^{-1}; respectively. The lines associated with the NH_2-scissoring modes (δ_{sNH2}) are predicted at 1617 (ν_9) and 1585 (ν_{10}) cm^{-1} for *ortho*-$HC_6H_5NH_2$, and at 1611 (ν_6) and 1601 (ν_7) cm^{-1} for *para*-$HC_6H_5NH_2$. In both cases, the former is a local NH_2-scissoring mode and the latter is coupled with a ring-deformation mode (δ_R). The lines associated with the NH_2-rocking modes (ρ_{NH2}) are predicted to be weak with IR intensity < 10 km mol^{-1}. Although the NH_2-wagging (inversion) modes (ω_{NH2}) are predicted to be intense, this result is likely a computational artifact, as discussed previously.[21] Because of a small inversion barrier for the NH_2 group, the NH_2-wagging mode is markedly anharmonic; its wavenumber and IR intensity cannot be predicted accurately with either harmonic or anharmonic (VPT2) vibrational analysis.

The lines of symmetric and antisymmetric CH_2-stretching modes (ν_{CH2}) are predicted at 2820 (ν_7) and 2791 (ν_8) cm^{-1}, respectively, for *ortho*-$HC_6H_5NH_2$, and at 2819 (ν_4) and 2796 (ν_5) cm^{-1} for *para*-$HC_6H_5NH_2$; the predicted IR intensities of these lines are > 30 km mol^{-1}. The lines associated with the CH_2-wagging mode (ω_{CH2}), 1252 (ν_{17}) cm^{-1} for *ortho*-$HC_6H_5NH_2$ and 1284 (ν_{10}) and 1165 (ν_{30}) cm^{-1}

for *para*-$HC_6H_5NH_2$, are predicted to be also intense. The line associated with the CH_2-rocking modes (ρ_{CH2}, ν_{25}) is weak in *ortho*-$HC_6H_5NH_2$ (with IR intensity ~2 km mol^{-1}) but is intense in *para*-$HC_6H_5NH_2$ (ν_{29} with IR intensity 63 km mol^{-1}). Other intense vibrational modes include the CH-stretching (ν_{CH}) and out-of-plane CH-bending (*oop* δ_{CH}) modes. The spectral ranges for the CH-stretching modes are 3033–3082 and 3028–3060 cm^{-1} for *ortho*- and *para*-$HC_6H_5NH_2$, respectively, which are near the range predicted for aniline 3044–3080 cm^{-1}. The intense lines associated with the out-of-plane CH-bending modes are predicted at 654 (ν_{30}) cm^{-1} for *ortho*-$HC_6H_5NH_2$ and at 949 (ν_{33}) cm^{-1} for *para*-$HC_6H_5NH_2$.

The characteristic vibrational modes mentioned above were predicted to be intense also for *meta*- and *ipso*-$HC_6H_5NH_2$, as listed in Tables S-1 and S-2. Overall, although similar vibrational modes are predicted to be intense among the four isomers, the predicted spectral patterns (vibrational wavenumbers and relative intensities) are sufficiently distinct for spectral identification.

4. EXPERIMETNAL RESULTS

Figure 3 shows representative IR spectra of an electron-bombarded $C_6H_5NH_2$/*p*-H_2 matrix in spectral ranges 1700–1100 and 1100–500 cm^{-1}; spectra in the NH- and CH_2-stretching regions, 3550–3340 and 2840–2680 cm^{-1}, are shown in Figure S-1. Figure 3(a) represents the spectrum measured after matrix deposition for 10 h; for clarity, the lines of aniline were subtracted using a spectrum of a $C_6H_5NH_2$/*p*-H_2 matrix deposited without electron bombardment. For some intense lines of aniline or lines slightly shifted upon electron bombardment, the subtraction was not clean; these regions are shaded with grey. After subtraction of lines of aniline, the remaining lines in this spectrum were induced upon electron bombardment. Figure 3(b) is a difference spectrum recorded after maintaining the electron-bombarded matrix in darkness for 19 h; the difference spectrum was obtained on subtracting the spectrum recorded before the experimental step from that recorded after the step so that positive lines indicate generation and negative ones indicate destruction. After this experimental step, the matrix was irradiated with light at 520 nm for 2 h, followed by irradiation with light at 465 nm for 10 min and at 375 nm for 10 min. Traces (c)–(e) show the difference spectra after each step of the

secondary photolysis.

An electron bombardment during matrix deposition of *p*-H_2 is known to produce H_3^+ and H atoms; proton transfer from H_3^+ and hydrogen addition to a guest molecule produce protonated and hydrogenated products, respectively.[11-12] The protonated products become slowly neutralized with electrons trapped in solid *p*-H_2. When we measured a spectrum after maintaining the matrix in darkness for a prolonged period, the intensities of lines of protonated products consequently decreased. The lines indicated with blue dots in trace (a) and showing corresponding negative lines in trace (b) have been assigned to three isomers of protonated aniline $H^+C_6H_5NH_2$; see Ref. 21 for details. In contrast, hydrogenated products are expected to increase after maintaining the electron-bombarded matrix in darkness for a prolonged period, because neutralization of protonated products produced their neutral counterparts and unreacted hydrogen atoms might further diffuse in solid *p*-H_2 to react with guest molecules. As a result, in the difference spectrum recorded after this step, trace (b), the positive lines might be associated with hydrogenated species. We identified two groups of lines that increased in this experimental step and labeled them A and B in Figure 3. The classification of these lines to groups A and B was established according to secondary photolysis experiments, in which distinct changes in intensity were observed for each group of lines. These lines in groups A and B are assigned to *ortho*-$HC_6H_5NH_2$ and *para*-$HC_6H_5NH_2$, respectively, to be discussed in Sections 5.1 and 5.2.

As shown in traces (b)–(e) of Figure 3 and summarized in Table 4, the intensities of lines in group A increased by (43±17) % during maintenance of the matrix in darkness for 19 h and decreased by (35±15), (13±8), and (75±10) % upon irradiation at 520, 465, and 375 nm, respectively; the percentage variations refer to the intensities recorded after deposition; the error limits represent one standard deviation for measurements of intense lines of group A at 1614.9, 1431.2, 1259.1, and 650.9 cm^{-1} and weaker ones at 1516.9 and 987.1 cm^{-1}. The intensities of lines in group B increased by (50±17) % during maintenance of the matrix in darkness for 19 h and decreased by (36±19), (30±19), and (19±5) % upon irradiation at 520, 465, and 375 nm, respectively. Intense lines of group B at 1606.0, 1455.7, 1290.4, 1263.8, 1035.8, and 521.9 cm^{-1} and weaker ones at 1588.3, 962.5, and 957.8 cm^{-1} were used in averaging. In the NH_2- and CH_2-stretching regions, four lines at 3482.3, 3406.7, 2770.8,

and 2713.7 cm^{-1} were identified to belong to group A; four lines at 3486.0, 3405.0, 2775.1, and 2706.1 cm^{-1} are identified to belong to group B. The correlations in intensity variations of these lines were, however, less satisfactory because of spectral interference from aniline and, in some cases, overlapping with lines in the other group.

5. DISCUSSION

5.1 Assignments of lines in group A to *ortho*-$HC_6H_5NH_2$

As discussed previously, the IR lines that were induced by electron bombardment and gained intensity during maintenance of the matrix in darkness are most likely due to hydrogenated species. To enable assignments of lines in groups A and B, we compared the experimental spectra in a representative region with the predicted spectra of four possible isomers of $HC_6H_5NH_2$ in Figure 4. The difference spectrum after secondary photolysis at 375 nm, which depleted lines in group A by ~75 % (and those in group B by only ~19 %), is inverted and presented in trace (a) so that the lines in group A, marked with blue squares, are pointing upward. The difference spectrum after the secondary photolysis at 465 nm, which depleted lines in group B by ~30 % (and those in group A by only ~13 %), is inverted and presented as trace (c), in which lines in group B are marked with red circles. Traces (b), (d), (e), and (f) are the stick IR spectra of *ortho*-, *para*-, *meta*-, and *ipso*-$HC_6H_5NH_2$, respectively, simulated according to the scaled harmonic vibrational wavenumbers and IR intensities predicted with the B3LYP/cc-pVTZ method.

In the spectral region below 1650 cm^{-1}, lines in group A were observed at 1614.9, 1516.9, 1431.2, 1259.1, 987.1, and 650.9 cm^{-1} (Figure 4(a)), in satisfactory agreement with the predicted spectrum of *ortho*-$HC_6H_5NH_2$, which has intense lines at 1617, (1585), 1518, 1428, 1252, 986, and 654 cm^{-1} (Figure 4(b)); see also Table 2. The line calculated at 1585 cm^{-1} (ν_{10}) is predicted to be intense enough (28 km mol^{-1}) but was unidentified in the experiment, likely because of interference from an unassigned line near 1583 cm^{-1}, of which the intensity varied differently from those in groups A and B; this line might be a perturbed line of the parent after electron bombardment. Observed and predicted wavenumbers for the NH_2-stretching mode also agree satisfactorily; the lines observed at 3482.3 and

3406.7 cm^{-1} correspond to those predicted at 3495 and 3399 cm^{-1} for the antisymmetric and symmetric NH_2-stretching modes. For the symmetric and antisymmetric CH_2-stretching modes, the lines observed at 2770.8 and 2713.7 cm^{-1} correspond to lines predicted at 2820 and 2791 cm^{-1}. These deviations are significantly greater than those of other lines but are characteristic of the harmonic vibrational calculations on CH_2-stretching modes of hydrogenated species. The anharmonic vibrational calculations indicate 2735 and 2703 cm^{-1} for these two modes of *ortho*-$HC_6H_5NH_2$, much smaller than those predicted from scaled harmonic vibrational calculations (Table 2); these deviations indicate that these modes are strongly coupled with other modes. We compared experimental values with scaled harmonic and anharmonic vibrational calculations of these two CH_2-stretching modes of several protonated aromatic compounds that we have studied in Table S-3; they all show a similar trend.

Based on the expected chemistry and the satisfactory agreement between predicted and observed spectra in terms of wavenumbers and relative intensities (Table 2), we assigned these ten lines in group A to *ortho*-$HC_6H_5NH_2$. The mean absolute deviation between scaled harmonic wavenumbers and observed wavenumbers is 16.5±24.5 cm^{-1}, in which the error represents one standard deviation in averaging; the average deviation decreases to 4.8±3.8 cm^{-1} when the lines of CH_2-stretching modes are excluded. The corresponding deviations from the anharmonic wavenumbers are 9.2±9.7 cm^{-1} and 5.7±4.1 cm^{-1}, respectively.

5.2 Assignment of lines in group B to *para*-$HC_6H_5NH_2$

In the spectral region below 1650 cm^{-1}, intense lines in group B were observed at 1606.0, 1455.7, 1290.4, 1263.8, and 521.9 cm^{-1} with intensities greater than 60 % of the most intense line at 1455.7 cm^{-1}; weaker lines were observed at 1588.3, 1035.8, 962.5, and 957.8 cm^{-1} (Figure 4(c)). These line positions and relative intensities are in satisfactory agreement with the spectrum predicted for *para*-$HC_6H_5NH_2$ (Figure 4(d)), of which intense lines are predicted at 1611, 1456, 1284, 1265, and 529 cm^{-1} with IR intensities > 45 km mol^{-1} and weaker ones are at 1601, 1037, 938, and 949 cm^{-1}. In this spectral region, all lines with predicted IR intensity > 7 km mol^{-1} were observed. In the NH_2-stretching region, the observed wavenumbers of lines in group B at 3486.0 and 3405.0 cm^{-1} agree satisfactorily

with those predicted at 3489 and 3397 cm^{-1} for the antisymmetric and symmetric NH_2-stretching modes. In the CH_2-stretching region, lines in group B were observed at 2775.1 and 2706.1 cm^{-1}, corresponding to the predicted scaled harmonic vibrational wavenumbers of 2819 and 2796 cm^{-1} for the symmetric and antisymmetric CH_2-stretching modes of *para*-$HC_6H_5NH_2$; similarly to *ortho*-$HC_6H_5NH_2$, the anharmonic vibrational wavenumbers 2714 and 2705 cm^{-1} for these two modes are much smaller than the scaled harmonic vibrational wavenumbers (Table 2).

Based on the expected chemistry and the satisfactory agreement between predicted and observed spectra in terms of wavenumbers and relative intensities (Table 3), we assigned these 14 lines in group B to *para*-$HC_6H_5NH_2$. The mean absolute deviation between scaled harmonic vibrational wavenumbers and observed wavenumbers is 15.7±23.4 cm^{-1}; the deviation decreases to 7.1±6.3 cm^{-1} when lines of CH_2-stretching modes are excluded. The corresponding values for the anharmonic vibrational wavenumbers are 13.6±15.2 cm^{-1} and 10.7±7.7 cm^{-1}, respectively

5.3 Behavior in secondary photolysis

To understand the behavior of secondary photolysis of these hydrogenated radicals $HC_6H_5NH_2$, we calculated their ultraviolet and visible absorption spectra with the TD-DFT method employing CAM-B3LYP/cc-pVTZ. The predicted vertical transitions, convoluted with Gaussian profiles of full width at half maximum (FWHM) 0.25 eV, are presented in Figure 5; actual absorption bands are expected to be red-shifted. In this figure, the wavelength regions used for secondary photolysis, 375±10, 465±10, and 520±10 nm, are indicated with violet, blue, and green rectangles, respectively. *ortho*-$HC_6H_5NH_2$ has intense absorption bands near 335 and 205 nm and weaker ones near 450 and 280 nm. The predicted spectrum of *para*-$HC_6H_5NH_2$ shows two intense absorptions near 280 and 220 nm and one moderately intense absorption centered near 515 nm. The predicted spectrum of *meta*-$HC_6H_5NH_2$ has three intense absorption bands near 210, 270, and 360 nm and one moderately intense absorption centered at 520 nm. *ipso*-$HC_6H_5NH_2$ has intense absorption bands near 225 and 310 nm with weaker ones near 225, 385, and 455 nm. Similarities among these spectra of various isomers of $HC_6H_5NH_2$ indicate that a wavelength that can dissociate only one isomer is unlikely to occur.

As summarized in Table 4, the irradiation at 375 nm significantly (by ~75 %) decreased the intensities of lines in group A (*ortho*-$HC_6H_5NH_2$), but only slightly (by ~19 %) the lines in group B (*para*-$HC_6H_5NH_2$), consistent with the predicted UV absorbance of *ortho*-$HC_6H_5NH_2$ much greater than that of *para*-$HC_6H_5NH_2$ near this region (Figure 5).

For the other two wavelengths, the photolytic behaviors of these two species are less distinct. Irradiation at 465 nm diminished *ortho*-$HC_6H_5NH_2$ by 13 %, but *para*-$HC_6H_5NH_2$ by 30%, consistent with a greater absorption cross section predicted for the latter in this region. However, irradiation at 520 nm decreased *ortho*- and *para*-$HC_6H_5NH_2$ by a similar fraction (~35%), even though the absorbance of *para*-$HC_6H_5NH_2$ was predicted to be about ten times that of *ortho*-$HC_6H_5NH_2$ at this wavelength. Considering that we are using only the predicted vertical excitations and convoluted with a fixed width, this deviation might be acceptable. Another possibility is that the excitation did not result into dissociation effectively. The key point is that the 375-nm wavelength is near the predicted main absorption band of *ortho*-$HC_6H_5NH_2$, which is mainly contributed by SOMO→LUMO and HOMO→LUMO transitions, whereas the corresponding absorption band of *para*-$HC_6H_5NH_2$ was predicted to have a smaller wavelength, so that significantly decreased IR lines of *ortho*-$HC_6H_5NH_2$ was observed near 375 nm.

5.4 Mechanism of formation

The mechanism for the formation of hydrogenated species upon electron bombardment of mixtures of *p*-H_2 and guest molecules has been discussed in the literature.[11-12] Briefly, electron bombardment ionizes H_2 molecule to produce H_2^+, which readily reacts with another H_2 molecule to produce H_3^+ and H atom. The H_3^+ and H are mobile in solid *p*-H_2 through exchange reactions with the nearby H_2 molecules. Proton transfer occurs to produce a protonated guest molecule if the proton affinity of the guest molecule is greater than that of H_2 (422 kJ mol^{-1}).[31] As aniline has a proton affinity of 882.5 kJ mol^{-1},[31] H_3^+ readily transfers a proton to aniline to form protonated aniline and H_2. The protonated aniline becomes neutralized by trapped electrons, which slowly diffuse in solid *p*-H_2, to produce hydrogenated species. The other process responsible for the generation of hydrogenated species is

hydrogen addition to aniline. The hydrogen additions to form *ortho*-, meta-, and *para*-$HC_6H_5NH_2$ have small barriers (Table 1), but these reactions can occur even at 3.2 K via quantum-mechanical tunneling.

Mixing ratios of products in solid *p*-H_2 are estimable according to the method developed by Tam and Fajardo.[32] Their method is based on Beer's law; the mixing ratio x (in ppm) in solid *p*-H_2 is represented as

$$x = \frac{2.303 \int \log_{10}(I/I_0)d\nu}{\varepsilon(\text{cm mol}^{-1})\, l(\text{cm})} \times V_m(\text{cm}^3\ \text{mol}^{-1}) \times 10^6, \quad (1)$$

in which ε is the absorption coefficient, $\int \log_{10}(I/I_0)d\nu$ is the observed integrated absorbance, l is the path length of IR light through solid *p*-H_2, and V_m (= 23.16 cm^3 mol^{-1})[33] is the molar volume of solid *p*-H_2. Infrared intensities calculated with the B3LYP/cc-pVTZ method were used for ε. The IR path length l was estimated from the integrated band area of transition $S_1(0) + S_0(0)$ of the *p*-H_2 matrix;[34-35] l is typically ~2 mm in these experiments. The major error in an estimate of this type is the error in calculated IR intensities, which might be as large as a factor of two. To minimize this error, we typically selected several lines of a species and averaged the estimated mixing ratio. Furthermore, on selecting similar vibrational modes of two species, we envisage that the relative error between these two species might cancel. To derive a definitive conclusion from quantitative analysis of the mixing ratios is difficult because of the associated large errors. However, the relative variations of each species in each experimental step are reliable.

The mixing ratios of observed protonated aniline isomers (*ortho*-, *para*-, and *amino*-$H^+C_6H_5NH_2$) and hydrogenated aniline isomers (*ortho*- and *para*-$HC_6H_5NH_2$) after matrix deposition and after maintenance in darkness for 19 h were estimated using several intense lines and the predicted IR intensities of each species. The estimated mixing ratios (in ppm) are summarized in Table 5. Just after the matrix deposition, the mixing ratios of $C_6H_5NH_2$, *ortho*- and *para*-$HC_6H_5NH_2$ are 53±5, 2.0±0.9 and 2.5±0.9, respectively; the error limits represent one standard deviation in averaging values derived from various absorption lines. The mixing ratios of *ortho*-, *para*-, and *amino*-$H^+C_6H_5NH_2$ are 0.6±0.1, 1.0±0.1, and 1.0±0.5, respectively, as reported previously;[21] because *para*-$H^+C_6H_5NH_2$ has a lower energy than *ortho*-$H^+C_6H_5NH_2$ by 18.4 kJ mol^{-1} according to the B3LYP/cc-pVTZ method, the barrierless formation of *para*-$H^+C_6H_5NH_2$ over *ortho*-$H^+C_6H_5NH_2$ is preferred. For the formation of

$HC_6H_5NH_2$ from H + $C_6H_5NH_2$, small barriers exist; the barriers to produce *ortho*- and *para*-$HC_6H_5NH_2$ are 9.8 and 11.3 kJ mol^{-1}, respectively; the energy of *para*-$HC_6H_5NH_2$ is greater than that of *ortho*-$HC_6H_5NH_2$ by 9.8 kJ mol^{-1}. Considering the barriers and relative energies, one would expect that *ortho*-$HC_6H_5NH_2$ might be slightly preferentially produced during deposition, from either neutralization of $H^+C_6H_5NH_2$ or hydrogenation of $C_6H_5NH_2$, but our observation indicated that the formation of *para*-$HC_6H_5NH_2$ might be slightly favored, 2.5±0.9 over 2.0±0.9, although within experimental uncertainties. This condition might also imply that the mixing ratio of *para*-$HC_6H_5NH_2$ was overestimated.

During maintenance of the matrix in darkness, hydrogenation can occur only via quantum-mechanical tunneling, so that the formation of *ortho*-$HC_6H_5NH_2$ is expected to be more efficient because of the smaller barrier. In contrast, formation of hydrogenated aniline via neutralization of protonated aniline is expected to depend only on the original mixing ratio of protonated species, if the neutralization involves no isomerization or dissociation; the formation of *para*-$HC_6H_5NH_2$ from neutralization is hence slightly preferred because of a greater mixing ratio of *para*-$H^+C_6H_5NH_2$.

After maintenance of the matrix in darkness for 19 h, we observed that the mixing ratios of *ortho*- and *para*-$HC_6H_5NH_2$ increased by 0.8±0.4 and 1.3±0.6 ppm, respectively; these values are ~40 and 52 % of the original ones. Even though the two uncertainty ranges overlap, the formation of *para*-$HC_6H_5NH_2$ appeared to be slightly favored. Furthermore, during this process, the estimated total loss of *para*- and *ortho*-$H^+C_6H_5NH_2$, 0.5±0.2 ppm, is smaller than the observed total production of *ortho*- and *para*-$HC_6H_5NH_2$, 2.1±1.4 ppm; the loss of aniline was estimated to be (5.4±2.6) ppm. Even though quantitative consistency was not achievable, these observations are consistent with an expectation that both neutralization of protonated aniline and hydrogenation of aniline occurred during the maintenance of the matrix in darkness. Even though the formation of *meta*-$HC_6H_5NH_2$ from H + $C_6H_5NH_2$ also has a small barrier and the energy of *meta*-$HC_6H_5NH_2$ is also small, we did not observe *meta*-$HC_6H_5NH_2$; this result seems to indicate that the hydrogenation is less important than neutralization during maintenance of the matrix in darkness, because *meta*-$H^+C_6H_5NH_2$ was not produced after electron bombardment due to its high energy, or the barrier for the formation of *meta*-$HC_6H_5NH_2$ from H +

$C_6H_5NH_2$ is actually larger than predicted. The absence of *meta*-$H^+C_6H_5NH_2$ might indicate that protonation on the *meta*-site is not the major channel of the Birch mechanism in this case.

Finally, we observed *amino*-$H^+C_6H_5NH_2$ but not its neutral counterpart $C_6H_5NH_3$, even though we expect the neutralization of *amino*-$H^+C_6H_5NH_2$ to occur. The reason is that, as $C_6H_5NH_3$ is unstable, neutralization of *amino*-$H^+C_6H_5NH_2$ might lead to a dissociation to $C_6H_5NH_2$ and H.

6. CONCLUSION

The two most stable isomers of hydrogenated aniline, *ortho*- and *para*-$HC_6H_5NH_2$, generated upon electron bombardment of a mixture of $C_6H_5NH_2$ and *p*-H_2 during matrix deposition, were identified with infrared spectroscopy. The IR spectra of these isomers of $HC_6H_5NH_2$ are new. The intensity of these IR lines increased during maintenance of the electron-bombarded matrix in darkness; they were classified into two groups (A and B) according to their intensity variations upon secondary photolysis at 520, 465, and 375 nm. The spectral assignments were made on comparison of observed wavenumbers and relative intensities with the vibrational wavenumbers and IR intensities predicted with the B3LYP/cc-pVTZ method. Ten lines in group A, of which the intensity decreased significantly upon irradiation at 375 nm and moderately at 520 and 465 nm, were assigned to the most stable *ortho*-$HC_6H_5NH_2$. Fourteen lines in group B, of which the intensities decreased moderately at all wavelengths employed, were assigned to *para*-$HC_6H_5NH_2$, which is predicted to have energy greater than *ortho*-$HC_6H_5NH_2$ by ~10 kJ mol^{-1}. The behavior of these species upon secondary photolysis was explained according to the UV-Vis spectra predicted with the TD-DFT method. Characteristic absorption lines of the CH_2-symmetric and CH_2-antisymmetric stretching modes were observed at 2770.8 and 2713.7 cm^{-1} for *ortho*-$HC_6H_5NH_2$ and 2775.1 and 2706.1 cm^{-1} for *para*-$HC_6H_5NH_2$.

The formation of these isomers is due partly to the neutralization of $H^+C_6H_5NH_2$ and, likely to a lesser extent, to the hydrogenation of aniline, according to the estimated variations of mixing ratios of isomers of $HC_6H_5NH_2$ and $H^+C_6H_5NH_2$.

ASSOCIAATED CONTENT

Supporting Information. Full lists of vibrational wavenumbers and IR intensities of *meta*-$HC_6H_5NH_2$ (Table S1) and *ipso*- $HC_6H_5NH_2$ (Table S2); comparison of experimental wavenumbers of CH_2-stretching modes in hydrogenated species (Table S3); and infrared spectra of an electron-bombarded $C_6H_5NH_2/p$-H_2 matrix in the region 2680–3550 cm^{-1} (Figure S1)

AUTHOR INFORMATION

Corresponding authors

* E-mail (MT): tsuge@lowtem.hokudai.ac.jp.

* E-mail (YPL): yplee@nctu.edu.tw.

Notes

The authors declare no competing financial interest.

ACKNOWLEDGMENT

This work was supported by Ministry of Science and Technology, Taiwan (grant numbers MOST108-2639-M-009-001-ASP and MOST108-3017-F009-004) and the Center for Emergent Functional Matter Science of National Chiao Tung University from The Featured Areas Research Center Program within the framework of the Higher Education Sprout Project by the Ministry of Education (MOE) in Taiwan. Japan Society for the Promotion of Science (JSPS KAKENHI grant number JP18K03717) partially supported this work. The National Center for High-Performance Computation of Taiwan and the Information Initiative Center of Hokkaido University provided computational resources.

References

1. Birch, A. J., Reduction by Dissolving Metals. Part I. *J. Chem. Soc.* **1944,** 430–436.
2. Zimmerman, H. E., A Mechanistic Analysis of the Birch Reduction. *Acc. Chem. Res.* **2012,** *45*, 164–170.
3. Watt, G. W., Reactions of Organic and Organometallic Compounds with Solutions of Metals in Liquid Ammonia. *Chem. Rev.* **1950,** *46*, 317–379.
4. Raphael, R. A., *Advances in Organic Chemistry*. Interscience Publishers: New York, 1972.
5. Birch, A. J.; Hinde, A. L.; Radom, L., A theoretical Approach to the Birch Reduction. Structures and Stabilities of Cyclohexadienyl Radicals. *J. Am. Chem. Soc.* **1980,** *102*, 4074–4080.

6. Birch, A. J.; Hinde, A. L.; Radom, L., A theoretical Approach to the Birch reduction. Structures and Stabilities of Cyclohexadienyl Anions. *J. Am. Chem. Soc.* **1980,** *102*, 6430–6437.

7. Zimmerman, H. E., Orientation in Metal Ammonia Reductions. *Tetrahedron* **1961,** *16*, 169–176.

8. Zimmerman, H. E.; Wang, P. A., The Regioselectivity of the Birch Reduction. *J. Am. Chem. Soc.* **1993,** *115*, 2205–2216.

9. Bahou, M.; Wu, Y.-J.; Lee, Y.-P., A New Method for Investigating Infrared Spectra of Protonated Benzene ($C_6H_7^+$) and Cyclohexadienyl Radical (*c*-C_6H_7) Using *para*-Hydrogen. *J. Chem. Phys.* **2012,** *136*, 154304.

10. DiGregorio, S.; Yim, M. B.; Wood, D. E., Electron Paramagnetic Resonance Study of Free Radicals in an Adamantane Matrix. VII. Aromatic Hydrogen Addition Radicals. *J. Am. Chem. Soc.* **1973,** *95*, 8455–8457.

11. Bahou, M.; Das, P.; Lee, Y.-F.; Wu, Y.-J.; Lee, Y.-P., Infrared Spectra of Free Radicals and Protonated Species Produced in *para*-Hydrogen Matrices. *Phys. Chem. Chem. Phys.* **2014,** *16*, 2200–2210.

12. Tsuge, M.; Tseng, C.-Y.; Lee, Y.-P., Spectroscopy of Prospective Interstellar Ions and Radicals Isolated in *para*-Hydrogen Matrices. *Phys. Chem. Chem. Phys.* **2018,** *20*, 5344–5358.

13. Raston, P. L.; Anderson, D. T., Infrared-induced Reaction of Cl Atoms Trapped in Solid Parahydrogen. *Phys. Chem. Chem. Phys.* **2006,** *8*, 3124–3129.

14. Tsuge, M.; Lai, C.-P.; Lee, Y.-P., Infrared Spectra of 3-hydroxy-(1H)-pyridinium Cation and 3-hydroxy-(1H)-pyridinyl Radical Isolated in Solid *para*-Hydrogen. *J. Chem. Phys.* **2018,** *149*, 014306.

15. Golec, B.; Das, P.; Bahou, M.; Lee, Y.-P., Infrared Spectra of the 1-Pyridinium ($C_5H_5NH^+$) Cation and Pyridinyl (C_5H_5NH and 4-C_5H_6N) Radicals Isolated in Solid *para*-Hydrogen. *J. Phys. Chem. A* **2013,** *117*, 13680–13690.

16. Bahou, M.; Wu, Y.-J.; Lee, Y.-P., Formation and Infrared Absorption of Protonated Naphthalenes (1-$C_{10}H_9^+$ and 2-$C_{10}H_9^+$) and their Neutral Counterparts in Solid *para*-Hydrogen. *Phys. Chem. Chem. Phys.* **2013,** *15*, 1907–1917.

17. Bahou, M.; Wu, Y.-J.; Lee, Y.-P., Infrared Spectra of Protonated Pyrene and its Neutral Counterpart in Solid *para*-Hydrogen. *J. Phys. Chem. Lett.* **2013,** *4*, 1989–1993.

18. Bahou, M.; Wu, Y.-J.; Lee, Y.-P., Infrared Spectra of Protonated Coronene and its Neutral Counterpart in Solid Parahydrogen: Implications for Unidentified Interstellar Infrared Emission Bands. *Angew. Chem. Int. Ed.* **2014,** *53*, 1021–1024.

19. Tsuge, M.; Bahou, M.; Wu, Y.-J.; Allamandola, L.; Lee, Y.-P., Infrared Spectra of Ovalene ($C_{32}H_{14}$) and Hydrogenated Ovalene ($C_{32}H_{15}$•) in Solid *para*-Hydrogen. *Phys. Chem. Chem. Phys.* **2016,** *18*, 28864–28871.

20. Sundararajan, P.; Tsuge, M.; Baba, M.; Sakurai, H.; Lee, Y.-P., Infrared Spectrum of Hydrogenated Corannulene *rim*-$HC_{20}H_{10}$ Isolated in Solid *para*-hydrogen. *J. Chem. Phys.* **2019,** *151*, 044304.

21. Tsuge, M.; Chen, Y.-H.; Lee, Y.-P., Infrared Spectra of Isomers of Protonated Aniline in Solid *para*-Hydrogen. *J. Phys. Chem. A* **2020,** *124*, 2253-2263.

22. Bahou, M.; Huang, C.-W.; Huang, Y.-L.; Glatthaar, J.; Lee, Y.-P., Advances in Use of *p*-H_2 as

a Novel Host for Matrix IR Spectroscopy. *J. Chin. Chem. Soc.* **2010,** *57*, 771–782.
23. Frisch, M. J.; Trucks, G. W.; Schlegel, H. B.; Scuseria, G. E.; Robb, M. A.; Cheeseman, J. R.; Scalmani, G.; Barone, V.; Mennucci, B.; Petersson, G. A.; et al. *Gaussian 09 Rev. E.01*, Wallingford CT, 2009.
24. Frisch, M. J.; Trucks, G. W.; Schlegel, H. B.; Scuseria, G. E.; Robb, M. A.; Cheeseman, J. R.; Scalmani, G.; Barone, V.; Petersson, G. A.; Nakatsuji, H.; et al. *Gaussian 16 Rev. B.01*, Wallingford, CT, 2016.
25. Becke, A. D., Density-functional Thermochemistry. III. the Role of Exact Exchange. *J. Chem. Phys.* **1993,** *98*, 5648–5652.
26. Lee, C. T.; Yang, W. T.; Parr, R. G., Development of the Colle-Salvetti Correlation-energy Formula into a Funcitional of the Electron-density. *Phys. Rev. B* **1988,** *37*, 785–789.
27. Dunning Jr., T. H., Gaussian-basis Sets for Use in Correlated Molecular Calculations. 1. The Atoms Boron through Neon and Hydrogen. *J. Chem. Phys.* **1989,** *90*, 1007–1023.
28. Bloino, J.; Barone, V., A Second-order Perturbation Theory Route to Vibrational Averages and Transition Properties of Molecules: General Formulation and Application to Infrared and Vibrational Circular Dichroism Spectroscopies. *J. Chem. Phys.* **2012,** *136*, 124108.
29. Bauernschmitt, R.; Ahlrichs, R., Treatment of Electronic Excitations within the Adiabatic Approximation of Time Dependent Density Functional Theory. *Chem. Phys. Lett.* **1996,** *256*, 454–464.
30. Yanai, T.; Tew, D. P.; Handy, N. C., A New Hybrid Exchange–correlation Functional Using the Coulomb-attenuating Method (CAM-B3LYP). *Chem. Phys. Lett.* **2004,** *393*, 51–57.
31. Hunter, E. P. L.; Lias, S. G., Evaluated Gas Phase Basicities and Proton Affinities of Molecules: An Update. *J. Phys. Chem. Ref. Data* **1998,** *27*, 413–656.
32. Tam, S.; Fajardo, M. E., Single and Double Infrared Transitions in Rapid-Vapor-Deposited Parahydrogen Solids: Application to Sample Thickness Determination and Quantitative Infrared Absorption Spectroscopy. *Appl. Spectrosc.* **2001,** *55*, 1634–1644.
33. Silvera, I. F., The Solid Molecular Hydrogens in the Condensed Phase: Fundamentals and Static Properties. *Reb. Mod. Phys.* **1980,** *52*, 393–452.
34. Fajardo, M. E., Matrix Isolation Spectroscopy in Solid Parahydrogen: A Primer. In *Physics and Chemistry at Low Temepratures*, Khriachtchev, L., Ed. Pan Stanford Publishing Pte. Ltd.: Singapore, 2011; pp 167–202.
35. Fajardo, M. E., Solid Parahydrogen Thickness Revisited. *Appl. Spectrosc.* **2019,** *73*, 1403–1408.

Table 1. Relative energies of isomers of mono-hydrogenated aniline $HC_6H_5NH_2$ and transition states for formation and isomerization reactions calculated with the B3LYP/cc-pVTZ method.[a]

isomer[b]	relative energy /kJ mol^{-1}	barrier for formation[c] /kJ mol^{-1}
ortho-	0.0	(9.8)
para-	9.8	(11.3)
meta-	14.2	(15.0)
ipso-	42.0	(38.3)
H + $C_6H_5NH_2$	103.8	
TS1 (*ortho-meta*)	195.8	
TS2 (*meta-para*)	204.8	
TS3 (*ipso-ortho*)	224.5	

[a] Zero-point vibrational energies are corrected using unscaled harmonic vibrational wavenumbers.

[b] See Figure 1 for hydrogenation sites.

[c] Energy of the transition state relative to that of H + $C_6H_5NH_2$.

Table 2. Comparison of observed vibrational wavenumbers (cm^{-1}) and IR intensities of lines in group A with scaled harmonic and anharmonic vibrational wavenumbers and relative IR intensities of *ortho*-$HC_6H_5NH_2$ predicted with the B3LYP/cc-pVTZ method.

ν_i	calculations		experiment	mode description[e]
	scaled harmonic[a,b]	anharmonic[c]	*p*-H_2[d]	
1	3495 (10)	3479 (13)	3482.3 (–)[f]	*a*-ν_{NH2}
2	3399 (10)	3393 (11)	3406.7 (–)[f]	*s*-ν_{NH2}
3	3082 (15)	3060 (34)	–[g]	ν_{C5H} + *s*-$\nu_{C3H}/\nu_{C4H}/\nu_{C6H}$
4	3063 (24)	3033 (54)	–[g]	*s*-ν_{C3H}/ν_{C4H} + ν_{C5H}
5	3045 (8)	3029 (17)	–[g]	*a*-ν_{C3H}/ν_{C4H} + ν_{C5H}
6	3033 (22)	3021 (42)	–[g]	ν_{C6H}
7	2820 (62)	2735 (133)	2770.8 (–)[f]	*s*-ν_{CH2}
8	2791 (54)	2703 (69)	2713.7 (7)	*a*-ν_{CH2}
9	1617 (100)	1617 (100)	1614.9 (100)	δ_{s}NH2
10	1585 (28)	1573 (55)	–[g]	δ_{s}NH2 + *s*-ν_{C3C4}/ν_{C1C6}
11	1518 (16)	1512 (16)	1516.9 (6)	*a*-ν_{C3C4}/ν_{C1C6}
12	1428 (30)	1421 (16)	1431.2 (39)	*a*-ν_{C1C2}/ν_{C5C6} + δ_{C6H} + δ_{s}CH2
13	1420 (7)	1412 (26)		*s*-ν_{C1C2}/ν_{C4C5} + δ_{s}CH2 + δ_{C4H}
14	1411 (2)	1409 (2)		*a*-ν_{C2C3}/ν_{C4C5} + $\delta_{C3H}/\delta_{C4H}$ + δ_{s}CH2
15	1339 (0)	1339 (1)		$\delta_{C3H}/\delta_{C4H}/\delta_{C5H}/\delta_{C6H}$ + ω_{CH2}
16	1291 (6)	1277 (7)		δ_R + ω_{CH2}
17	1252 (63)	1252 (28)	1259.1 (39)	ν_{C1N} + δ_R + ω_{CH2}
18	1168 (1)	1172 (17)		t_{CH2}
19	1160 (0)	1167 (0)		*a*-$\delta_{C3H}/\delta_{C4H}$
20	1123 (4)	1126 (16)		*a*-$\delta_{C5H}/\delta_{C6H}$
21	1076 (1)	1076 (2)		ρ_{NH2} + *s*-ν_{C1C2}/ν_{C4C5}
22	986 (9)	989 (10)	987.1 (4)	δ_R
23	961 (1)	960 (1)		δ_R
24	940 (1)	940 (1)		*oop* (δ_{C4H} + *s*-$\delta_{C3H}/\delta_{C5H}$)
25	934 (2)	929 (5)		*oop* δ_{C3H} + ρ_{CH2}
26	915 (6)	918 (8)		δ_R
27	862 (11)	871 (7)		*oop* (δ_{C5H} + δ_{C6H})
28	767 (1)	769 (3)		ring breathing
29	725 (1)	742 (3)		*oop a*-$\delta_{C3H}/\delta_{C5H}$
30	654 (84)	653 (85)	650.9 (44)	*oop s*-$\delta_{C3H}/\delta_{C4H}/\delta_{C5H}$
31	582 (4)	580 (9765)		δ_R
32	577 (231)	426 (688)		ω_{NH2} (inversion)
33	531 (9)	530 (65)		*oop* δ_R
34	492 (11)	491 (69)		δ_R
35	459 (39)	453 (160)		*oop* δ_R + ω_{NH2}

36	381	(5)	366	(5)	δ_{CCN}
37	346	(32)	317	(103)	τ_{CN}
38	275	(4)	268	(6)	*oop* δ_R
39	135	(0)	118	(1)	*oop* δ_R

[a] Scaled with equations $y = 0.9212\ x + 138$ and $y = 0.9716\ x + 8.5$ for values above and below 2000 cm^{-1}, respectively; y is the scaled vibrational wavenumber and x is the calculated harmonic vibrational wavenumber; see text for details.

[b] Predicted percentage IR intensities relative to the intensity of the ν_9 line, 106 km mol^{-1}, are listed in parentheses.

[c] Predicted percentage IR intensities relative to the intensity of the ν_9 line, 61 km mol^{-1}, are listed in parentheses

[d]. Percentage integrated IR intensities relative to the most intense line at 1614.9 cm^{-1} (ν_9) are listed in parentheses.

[e] Approximate mode descriptions. ν: stretch, δ: bend or deformation, δ_R: ring deformation, δ_s: scissor, ρ: rock, ω: wag, *t*: twist, τ: torsion, *a*: antisymmetric, *s*: symmetric, *oop*: out-of-plane.

[f] Indeterminate because of significant interference from absorption of the parent or other lines.

[g] Unidentifiable definitively because of significant interference from absorption of the parent or other lines.

Table 3. Comparison of observed vibrational wavenumbers (cm^{-1}) and IR intensities in group B with scaled harmonic and anharmonic vibrational wavenumbers and relative IR intensities of *para*-$HC_6H_5NH_2$ predicted with the B3LYP/cc-pVTZ method.

ν_i	sym.	calculations			experiment	mode description[e]
		scaled harmonic[a,b]		anharmonic[c]	*p*-H_2[d]	
1	*a′*	3397	(18)	3383 (10)	3405.0 (27)	*s*-ν_{NH2}
2	*a′*	3060	(5)	3037 (35)		*s*-(ν_{C3H}/ν_{C5H} + ν_{C2H}/ν_{C6H})
3	*a′*	3029	(45)	2983 (73)	–[f]	*s*-(ν_{C2H}/ν_{C6H}) – *s*-(ν_{C3H}/ν_{C5H})
4	*a′*	2819	(181)	2714 (282)	2775.1 (–)[g]	*s*-ν_{CH2}
5	*a′*	2796	(75)	2705 (158)	2706.1 (9)	*a*-ν_{CH2}
6	*a′*	1611	(157)	1608 (130)	1606.0 (64)	δ_{s}NH2
7	*a′*	1601	(17)	1587 (70)	1588.3 (17)	*s*-ν_{C2C3}/ν_{C5C6}+ δ_{s}NH2
8	*a′*	1456	(100)	1451 (100)	1455.7 (100)	δ_R + δ_{s}CH2 + δ_{C2H}/δ_{C3H}/δ_{C5H}/δ_{C6H}
9	*a′*	1424	(1)	1414 (1)		δ_{s}CH2
10	*a′*	1284	(113)	1286 (71)	1290.4 (71)	ν_{C1N} +δ_R
11	*a′*	1174	(11)	1175 (27)		*a*-δ_{C2H}/δ_{C3H} + *a*-δ_{C5H}/δ_{C6H}
12	*a′*	967	(2)	978 (5)		δ_R
13	*a′*	938	(11)	937 (9)	962.5 (8)	ρ_{CH2} + *oop*-δ_{C3H}/δ_{C5H}
14	*a′*	919	(20)	924 (34)	911.7 (12)	*oop* (*s*-δ_{C2H}/δ_{C3H} – *s*-δ_{C5H}/δ_{C6H})
15	*a′*	865	(9)	868 (22)		δ_R
16	*a′*	767	(5)	761 (32)		δ_R (breathing)
17	*a′*	707	(122)	708 (90)		*oop* δ_{C3H}/δ_{C5H}
18	*a′*	619	(641)	505 (812)		ω_{NH2} (inversion)
19	*a′*	529	(116)	534 (234)	521.9 (66)	*oop* δ_{C2H}/δ_{C3H}/δ_{C5H}/δ_{C6H} + ρ_{CH2}
20	*a′*	495	(1)	493 (8)		δ_R
21	*a′*	277	(17)	282 (23)		*oop* δ_R
22	*a′*	119	(3)	119 (3)		*oop* δ_R + ρ_{CH2}
23	*a″*	3489	(23)	3466 (22)	3486.0 (29)	*a*-ν_{NH2}
24	*a″*	3058	(69)	3020 (123)	–[f]	*a*-ν_{C3H}/ν_{C5H} + *a*-ν_{C2H}/ν_{C6H}
25	*a″*	3028	(33)	3021 (88)	–[f]	*a*-(ν_{C2H}/ν_{C6H}) – *a*-(ν_{C3H}/ν_{C5H})
26	*a″*	1516	(9)	1507 (7)		*a*-ν_{C2C3}/ν_{C5C6}
27	*a″*	1392	(7)	1388 (13)		δ_R + ω_{CH2}
28	*a″*	1336	(0)	1333 (0)		δ_{C2H}/δ_{C3H}/δ_{C5H}/δ_{C6H} + ω_{CH2}
29	*a″*	1265	(138)	1254 (161)	1263.8 (70)	δ_R + ω_{CH2}
30	*a″*	1165	(0)	1159 (0)		t_{CH2}
31	*a″*	1152	(3)	1158 (4)		*a*-δ_{C2H}/δ_{C3H}/δ_{C5H}/δ_{C6H} + ω_{CH2}
32	*a″*	1037	(47)	1043 (51)	1035.8 (34)	ρ_{NH2}
33	*a″*	949	(56)	951 (59)	957.8 (18)	δ_R + ω_{CH2}
34	*a″*	926	(1)	932 (0)		*oop* δ_{C2H}/δ_{C3H}/δ_{C5H}/δ_{C6H}
35	*a″*	699	(0)	705 (0)		*oop* δ_{C2H}/δ_{C3H}/δ_{C5H}/δ_{C6H}

36	*a″*	604	(2)	606 (3)	δ_R
37	*a″*	389	(0)	386 (0)	*oop* δ_R
38	*a″*	362	(3)	364 (2)	δ_{CCN}
39	*a″*	258	(32)	295 (45)	τ_{CN}

[a] Scaled with equations $y = 0.9212\ x + 138$ and $y = 0.9716\ x + 8.5$ for values above and below 2000 cm^{-1}, respectively; y is the scaled vibrational wavenumber and x is the calculated harmonic vibrational wavenumber; see text for details.

[b] Predicted percentage IR intensities relative to the intensity of the ν_8 line, 46 km mol^{-1}.

[c] Predicted percentage IR intensities relative to the intensity of the ν_8 line, 30 km mol^{-1}.

[d] Percentage integrated IR intensities relative to the most intense line at 1455.7 cm^{-1} (ν_8) are listed in parentheses.

[e] Approximate mode descriptions. ν: stretch, δ: bend or deformation, δ_R: ring deformation, δ_s: scissor, ρ: rock, ω: wag, *t*: twist, τ: torsion, *a*: antisymmetric, *s*: symmetric, *oop*: out-of-plane.

[f] Unidentifiable definitively because of significant interference from absorption of the parent or other lines.

[g] Indeterminate because of significant interference from absorption of a line in group A.

Table 4. Variation of spectral intensities of lines in groups A and B at each stage of experiments.

group	in darkness	secondary photolysis		
	19 h	520 nm	465 nm	375 nm
A	+(43±17)[a] %	−(35±15)[a] %	−(13±8)[a] %	−(75±10)[a] %
B	+(50±17) %	−(36±19) %	−(30±19) %	−(19±5) %

[a] The percentage variations are the integrated intensities of lines relative to those in the IR spectrum recorded just after matrix deposition (Figure 3(a)); values from several representative lines in each group are averaged, as described in the text. The errors represent one standard deviation in averaging several representative lines in each group.

Table 5. Estimated mixing ratios (in ppm) of isomers of protonated and hydrogenated aniline.

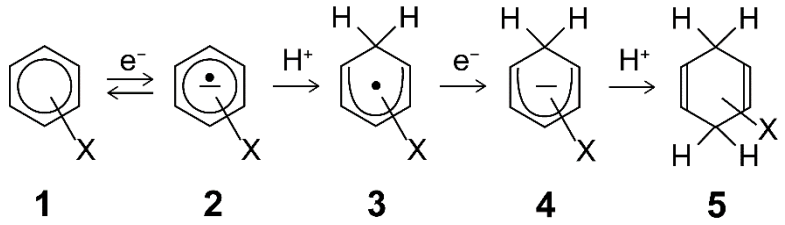
isomer [a]	hydrogenated aniline		protonated aniline	
	after deposition[b]	19 h in darkness[c]	after deposition[b]	19 h in darkness[c]
ortho-	2.0±0.9	+(0.8±0.4)	0.6±0.1	−(0.2±0.1)
para-	2.5±0.9	+(1.3±0.6)	1.0±0.1	−(0.3±0.1)
amino-	–	–	1.0±0.5	−(0.3±0.2)
sum[d]	4.5±1.9	+(2.1±1.0)	2.6±0.7	−(0.9±0.4)

[a] The mixing ratio of aniline was estimated to be (53±5) ppm after deposition; it was diminished by (5.4±2.6) ppm after maintenance of the matrix in darkness for 19 h.

[b] Estimated from the spectra shown in Figure 3(a) and predicted harmonic IR intensities according to the method of Tam and Fajardo;[32] see the text for details. The errors represent one standard deviation in averaging several representative lines of each species.

[c] Variations in mixing ratios after this experimental process are shown.

[d] Sum of mixing ratios of all observed isomers.



Scheme 1. Mechanisms of the Birch reduction of substituted benzene; the substituent (X) is an electron-donating group.

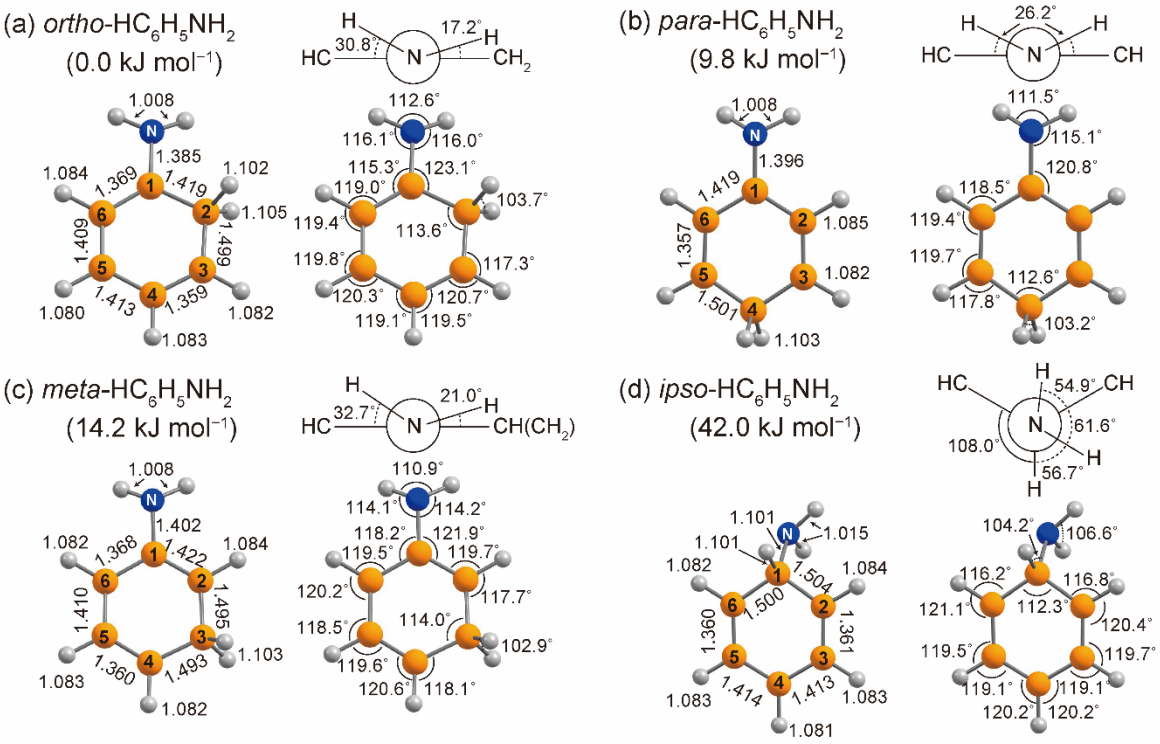


Figure 1. Geometries of (a) *ortho*-$HC_6H_5NH_2$, (b) *para*-$HC_6H_5NH_2$, (c) *meta*-$HC_6H_5NH_2$, and (d) *ipso*-$HC_6H_5NH_2$ optimized with the B3LYP/cc-pVTZ method. The ZPVE-corrected energies (in kJ mol^{-1}) are listed in parentheses. For each species, bond lengths in Å are indicated on the left and bond angles in degree on the right. Dihedral angles are indicated with Newman diagrams. *para*-$HC_6H_5NH_2$ belongs to symmetry point group C_s and others belong to symmetry point group C_1.

(double column)

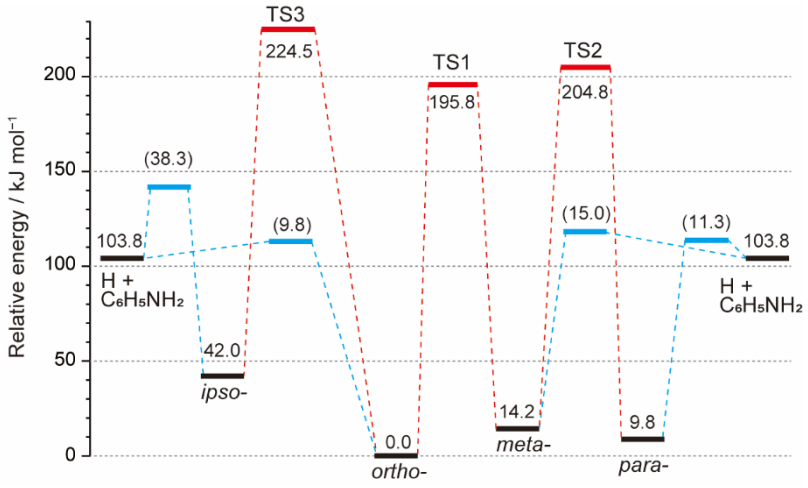


Figure 2. Energy diagram representing the relative energies of hydrogenated aniline isomers (*ortho*-, *para*-, *meta*-, and *ipso*-$HC_6H_5NH_2$) and transition states for formation and isomerization. Blue lines indicate hydrogen-addition reactions with barriers indicated in parentheses, and red lines indicate isomerization reactions. Calculations were performed with the B3LYP/cc-pVTZ method; ZPVE were corrected with unscaled harmonic wavenumbers. The relative energies are summarized in Table 1.

(1.5 column)

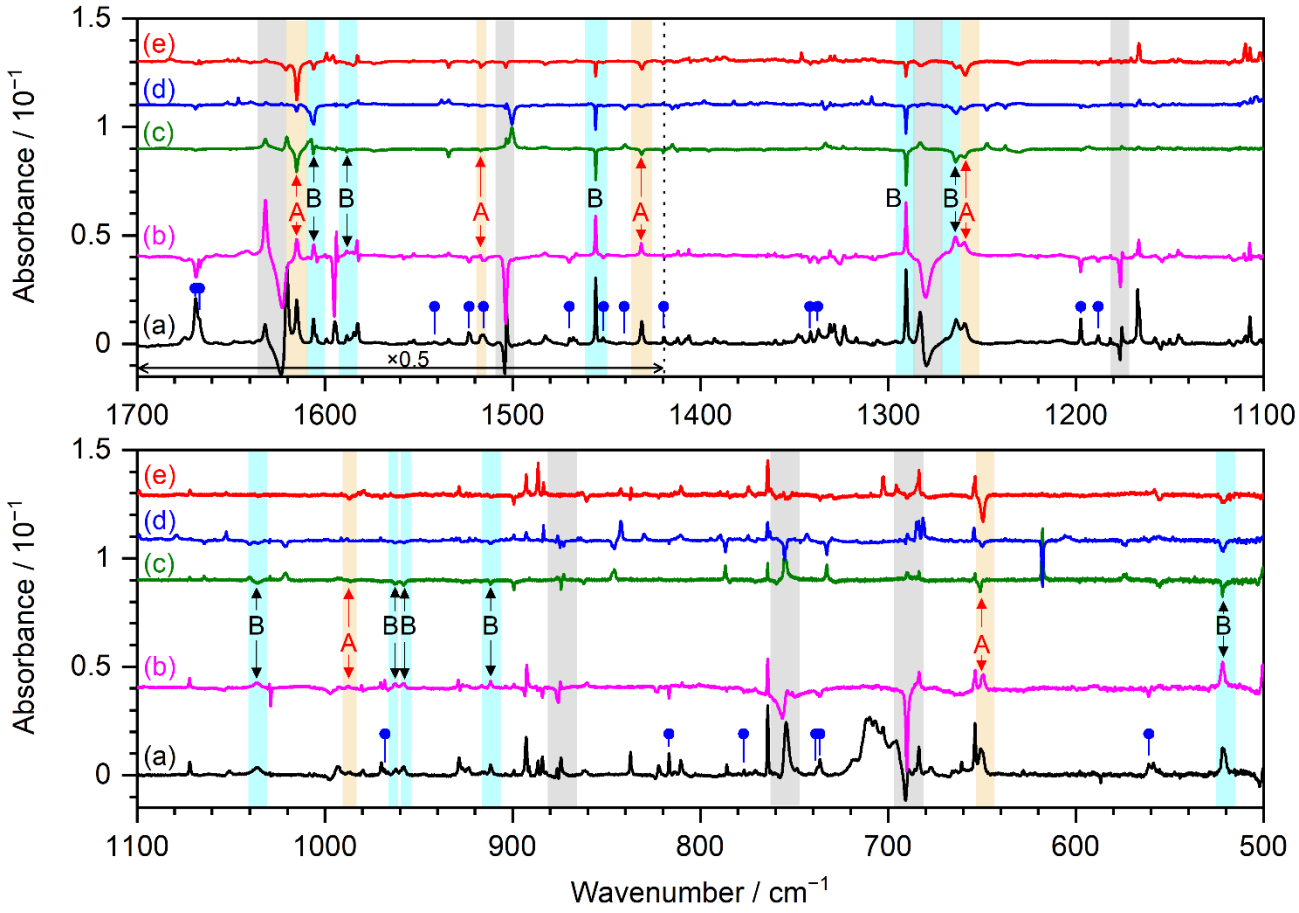


Figure 3. Representative IR spectra of an electron-bombarded $C_6H_5NH_2$/*p*-H_2 matrix after each experimental step. (a) After deposition at 3.2 K for 10 h; the lines of $C_6H_5NH_2$ were stripped using a spectrum measured for a $C_6H_5NH_2$/*p*-H_2 matrix prepared without electron bombardment. (b) Difference spectrum of the matrix after maintenance in darkness for 19 h. (c) Difference spectrum after further secondary photolysis at 520 nm for 2 h. (d) Difference spectrum after secondary photolysis at 465 nm for 10 min. (e) Difference spectrum after secondary photolysis at 375 nm for 10 min. The secondary photolysis was performed sequentially. The lines in groups A and B are indicated with levels and highlighted with light-skin-color and light-blue rectangles, respectively. The regions shaded with grey are interfered by intense lines of parent ($C_6H_5NH_2$). In (a), the lines assigned to protonated aniline isomers (*para*-, *amino*-, or *ortho*-$C_6H_5NH_2$) are indicated with blue dots.

(double column)

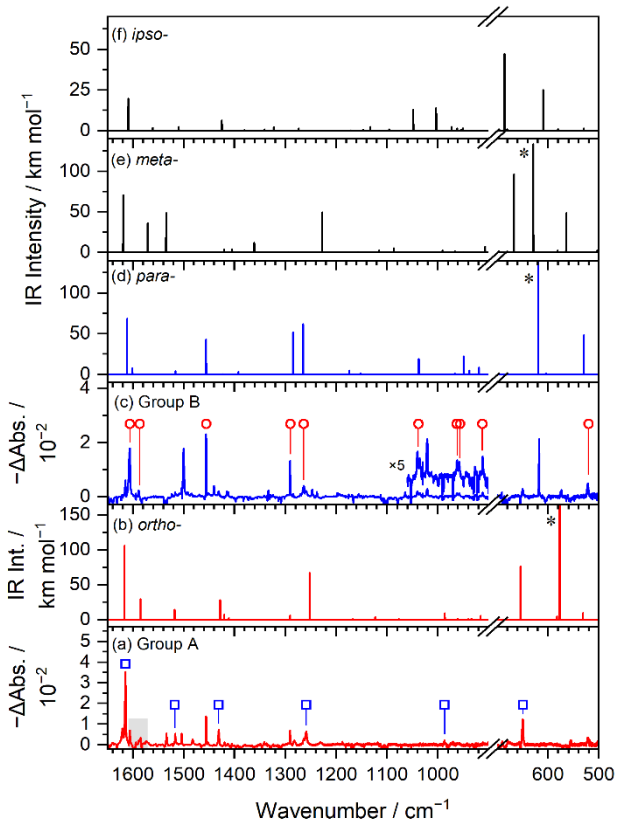


Figure 4. Comparison of experimental results with predicted IR spectra of various isomers of $HC_6H_5NH_2$. (a) Difference spectrum upon secondary photolysis at 375 nm for 10 min; taken from Figure 3(e) and inverted. The lines in group A are indicated with blue squares. The region suffering from interference is shaded with grey. (b) Predicted stick spectrum of *ortho*-$HC_6H_5NH_2$. (c) Difference spectrum upon secondary photolysis at 465 nm for 10 min; taken from Figure 3(d) and inverted. The lines in group B are indicated with red circles. (d)–(f) Predicted stick spectra of *para*-, *meta*-, and *ipso*-$HC_6H_5NH_2$, respectively. Predicted spectra were simulated according to scaled harmonic wavenumbers and IR intensities predicted with the B3LYP/cc-pVTZ method. Predicted lines marked with * are associated with the NH_2-wagging (or inversion) modes, of which predictions are difficult with a harmonic vibrational analysis.

(single column)

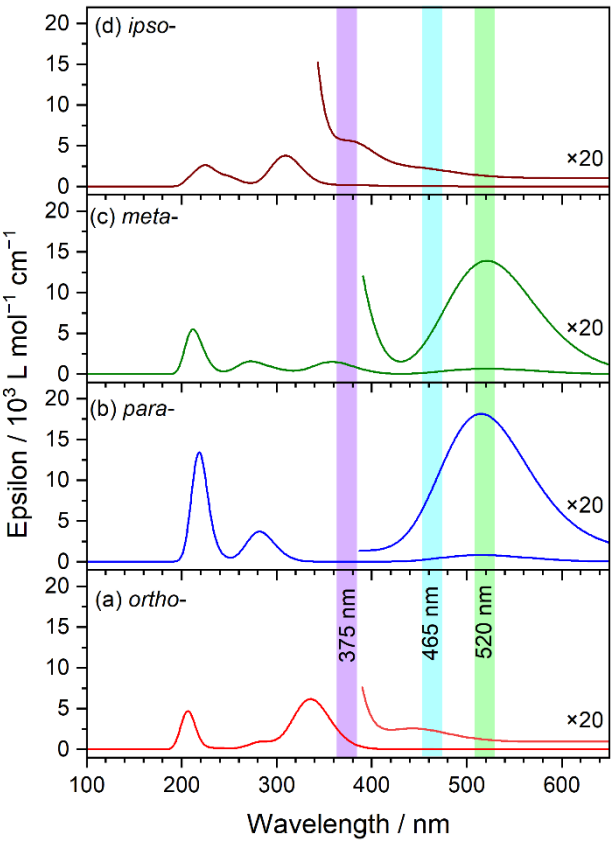


Figure 5. Predicted UV-Vis absorption spectra of (a) *ortho*-$HC_6H_5NH_2$, (b) *para*-$HC_6H_5NH_2$, (c) *meta*-$HC_6H_5NH_2$, and (d) *ipso*-$HC_6H_5NH_2$ predicted with the TD-CAM-B3LYP/cc-pVTZ method. Predicted transitions are convoluted with Gaussian profiles of FWHM 0.25 eV. The wavelength ranges used for secondary-photolysis experiments (375 nm, 465 nm, and 375 nm) are indicated with violet, blue, and green rectangles, respectively.

(single column)